Supplementary Material for

**Missing water from the Qiantang Basin on the Tibetan Plateau**

Bin Yong[1], Chi-Yuen Wang[2], Jiansheng Chen[3*], Jiaqi Chen[4], D. A. Barry[5], Tao Wang[6], Ling Li[7*]

*Corresponding authors: jschen@hhu.edu.cn; liling@westlake.edu.cn

**This file includes:**

Materials and Methods

Figures S1 to S6

Data availability

Caption for data S1

References (31-57)

**Other supplementary material for this manuscript include:**

Dataset S1 (Source Data with Excel file for generating the figures)

## Materials and Methods

The supplementary material is composed of seven text sections, six supplementary figures, data availability, added references, and source data with Excel file. Some important supplementary information, mainly including fundamental theory, calculating methods, modelling experiments, data processing and uncertainty analysis, are described in details.

### 1. Atmospheric water balance equation of a hydrologic unit ($P – E = I – O$)

With the atmosphere of a basin taken as a control volume (Fig. 1B), the water balance (WMO/IHD Projects Report, 1973) within this volume is,

$$\frac{\partial Wa}{\partial t} = (I + E) - (O + P) \tag{3}$$

where $I$ and $O$ are the vapour fluxes into and out of the atmospheric control volume, respectively. $P$ and $E$ are precipitation and evapotranspiration rates, respectively. $W_a$ is the total amount of water vapour stored in the atmosphere volume.

Given that $W_a$ does not change much over a monthly or yearly time scale for the long-time average, i.e., $\frac{\partial Wa}{\partial t} \approx 0$, Eq. 3 leads to:

$$I - O = P - E \tag{4}$$

Equation 4 simply represents the balance between the net water vapour flux to the atmosphere of a hydrological unit and the net atmosphere-land exchange given by $P – E$ under the quasi-steady state condition over the monthly or yearly time scale.

### 2. Application of GLDAS with validation of precipitation estimates in the Qiangtang Basin

As a powerful land surface modelling system developed jointly by NASA, GSFC, NOAA and NCEP, GLDAS integrates satellite- and ground-based observational data products and

adopts advanced land surface modelling and data assimilation to generate optimal fields of land surface states and fluxes (Rodell et al., 2004). For GLDAS Version 1.0, the developers found that the precipitation estimates are subjected to low biases relative to the Global Precipitation Climatology Project (GPCP) dataset (Rui and Beaudoing, 2018). In GLDAS Version 2.0, the precipitation fields were disaggregated using the GPCP and TRMM datasets. In the latest GLDAS Version 2.1, the GPCP 1-degree Daily dataset (Huffman et al., 2001) is incorporated and an updated disaggregation routine (making use of the Global Data Assimilation System of NCEP [Deber et al., 1991]) is adopted to further improve predictions of the precipitation fields. Here we use the field of total precipitation rate in GLDAS including rain and snow precipitation to evaluate the water balance of the Qiangtang Basin. The data based on GLDAS Noah V2.1 (Rodell et al., 2004) accounts for the needed spatial resolution and time series span. This GLDAS dataset provides monthly precipitation and evapotranspiration estimates of quasi-global land surface at relatively fine resolution ($0.25^{\circ} \times 0.25^{\circ}$) from 2000 onwards (Rui and Beaudoing, 2018), which covers the 15 years (2002-2016) time span of the GRACE observations (Rodell et al., 2018).

In this study, therefore, we employed the latest GLDAS (Version 2.1) to compute precipitation ($P$) and evapotranspiration ($E$) of the Qiangtang Basin on grids of $0.25^{\circ} \times 0.25^{\circ}$. To assess and validate the accuracy of estimated precipitation by GLDAS, we used five sets of TRMM-based mainstream multi-satellite precipitation products (TMPA [Huffman et al., 2007], CMORPH [Joyce et al., 2004], GSMaP [Sorooshian et al., 2000], PERSIANN [Kubota et al., 2000] and ITPCAS [Chen et al., 2011]) for comparison with GLDAS results at a monthly scale. The monthly precipitation data of nine rainfall gauges during the summer of 2008 are used as the ground truth (refer to Table 1 in Zhou et al., [2013]). These gauges are distributed around Lake Namtso in the southeast part of the Qiangtang Basin, where the

precipitation rate is the highest across the whole basin. Note that the Qiangtang Basin is a very remote, ungauged region with very few ground truth data available.

Figure S1 shows that the GLDAS precipitation estimates match the measured data most closely with the highest correlation (correlation coefficient, $CC = 0.77$) and lowest errors (e.g., $BIAS = -8.19\%$), outperforming all the multi-satellite precipitation products. The results provide confidence in the precipitation estimates by GLDAS. Further validation of the GLDAS results, combining $P$ and $E$ as $P - E$, is provided below.

**Insert Figure S1 near here**

**3. Application of GARA for estimating the vapour fluxes in order to further validate the GLDAS results: Validation of GLDAS-derived $P - E$ using GARA-estimated $I - O$**

Qiangtang is the highest and largest ungauged endorheic basin in the world. No ground measurement data are available for determining evapotranspiration rates ($E$) for validating the estimates of $E$ by GLDAS. Instead we use Global Atmospheric Reanalysis (GARA) to calculate $I$ and $O$ to the atmosphere above the Qiangtang Basin. The net vapour flux $I - O$ is then compared with $P - E$ over the basin to cross-check both results against the balance principle as given by Eq. 4. Two widely-used GARA datasets (ERA-Interim and JRA-55) are normally considered as the optimal global atmosphere reanalysis with fine-quality and high-precision due to their powerful data assimilation systems and rich data sources. In our study, both ERA-Interim (Dee et al., 2011; with time steps of 6 h and spatial grids of $1^\circ \times 1^\circ$) and JRA-55 (Kabayashi et al., 2015; with time steps of 6 h and spatial grids of $1.25^\circ \times 1.25^\circ$) data are used to compute the water vapour fluxes, i.e, $I$ and $O$.

The specific horizontal water vapour flux over the whole air column for a unit length of the hydrological unit boundary, $Q$ (kg m$^{-1}$ s$^{-1}$), is given by (Starr and White, 1954; Liu and Zhou, 1985)

$$Q = g^{-1} \int_{pt}^{ps} q\vec{V} \, dp \tag{5}$$

where $g$ is the magnitude of gravity acceleration (m s$^{-2}$), $\vec{V}$ denotes the wind velocity perpendicular to the boundary (m s$^{-1}$), $q$ is specific humidity (kg kg$^{-1}$), and $p$ represents the atmospheric pressure (hPa), with $pt$ and $ps$ being the land surface air pressure (1000 hPa assumed in our calculations) and air pressure at the top of the air column (200 hPa), respectively. Note that $Q$ (vector) is typically decomposed into the longitudinal component ($Q_\lambda$) and latitudinal component ($Q_\varphi$). ERA-Interim and JRA-55 provide all parameter values for computing $Q$ using Eq. 5 (Berrisford et al., 2011; JRA-55 Product User′ handbook, 2013). $Q$ can then be integrated along the boundary of the hydrological unit to determine the total water vapour flux into or out of the atmosphere above.

The results for the Qiangtang Basin as the hydrological unit show very good agreement among the $P - E$ values estimated by GLDAS, and the $I - O$ values given by both ERA-Interim and JRA-55 on the monthly time scale (see Fig. 2C).

## 4. Estimation of water leakage from Qiangtang Basin using the GLDAS data ($P - E$) and GRACE data ($\Delta S$)

Considering the dynamic changes of terrestrial water components including groundwater, soil moisture, surface waters (e.g., lakes and rivers), snow and ice, we used the monthly GRACE data (Rodell and Famiglietti, 1999; Rodell et al., 2018) to estimate the changes of terrestrial water storage (TWS; the sum of these five components). Since its launch in 2002, the GRACE satellites provide a direct monthly estimate for the total TWS changes due to, for example, ice-sheet and glacier ablation, groundwater depletion and surface water increase or

decrease (Rodell and Famiglietti, 1999; Tapley et al., 2004; Cazenave et al., 2010; Rodell et al., 2018; Scanlon et al., 2018). Three GRACE mission's partner centres, including the University of Texas Center for Space Research (CSR), the NASA Jet Propulsion Laboratory (JPL) and the Deutsches GeoForschungsZentrum (GFZ), provide independent monthly time-variable gravity field solutions, respectively (Swenson, 2012; Jean et al., 2018). Even though CSR, JPL and GFZ use the same GRACE raw data for computing the monthly solutions, there are still significant differences among them, which translate to differences in the TWS fields (Ferreira et al., 2016). Hence, here we use an ensemble mean (Sakumura et al., 2014) based on the solutions of each centre at the monthly scale over grids of $1° \times 1°$. Since there are some missing solutions during the GRACE time-span from April 2002 to May 2017, the averaged surface mass density for the Qiangtang Basin for the respective missing periods were estimated through interpolation between those of the previous and next months (Ramillien et al., 2016). Furthermore, cross-validation showed that this method presents a root-mean-square error of less than 20.0 kg m$^{-2}$ as reported in previous studies (Andam-Akorful et al., 2015). Results from our analysis indicate that little change occurred to the long-term average TWS ($\Delta S$ of 0.06±14.17 km$^3$ yr$^{-1}$) for the entire Qiangtang Basin over the period from May 2002 to December 2016.

So far, we have estimated the crucial components ($P - E$ and $\Delta S$) of the water budget for the Qiangtang Basin. Thus, the water leakage can be computed as $P - E - \Delta S$ since no rivers flow into or out of the endorheic (closed) Qiangtang Basin (i.e., $R = 0$). Figure S2 shows the time series of the water balance components estimated by GLDAS and GRACE for the basin. The seasonality of Qiangtang is bi-annual with a warm season from May to September and a cold season from October to next April. The results show that annually 84.17% of the leakage occurs in the warm months (Fig. S2G) on average. Increased precipitation in these months led to significant rise in the leakage (Fig. S2F). Over the whole period considered (2002-2016),

the average annual leakage estimated by the GLDAS and GRACE data across the entire basin amounted to 54.52 $km^3$ $yr^{-1}$.

**Insert Figure S2 near here**

## 5. Uncertainty analysis in calculating the averaged annual water leakage (*L*) by nine groups of modelling experiments

In our study, the water balance calculation mainly relies on a synergy of multimodel ensemble and satellite observations due to limited ground measurements over the poorly gauged plateau basin. In terms of currently operational models, GLDAS, ERA-Interim and JRA-55 can provide optimal field of water fluxes (e.g., *P*, *E*, *I* and *O*) between the land and atmosphere since their systems ingested numerous satellite- and ground-based observational data and employed advanced modelling and assimilation approaches. Moreover, these three models are independent of each other owing to using different data sources and integrating algorithms. Thus, they were selected to calculate *P – E* or *I – O* of the entire Qiangtang Basin, and then perform the multimodel ensemble in this study. On the other hand, it is considered that GRACE has presently become the only practical way to measure the changes of terrestrial water storage at the large scale. Hence, in our analysis, we selected three widely-used GRACE solutions (i.e., CSR, JPL and GFZ), which can provide independent and monthly time-variable gravity field, to estimate annual terrestrial water storage change (*ΔS*) of the basin.

To ensure the credibility of water balance calculations, we designed nine groups of modelling experiments (3 models × 3 GRACE solutions) to estimate the averaged annual water leakage (*L*) from 2002 to 2016 of the entire Qiangtang Basin (see Fig. S3). First, we combined GLDAS and three GRACE satellite solutions (CSR, JPL and GFZ), respectively, to calculate annual water leakage (*L = P – E – ΔS*; refer to red circles in Fig. S3). Subsequently, the

annual water leakage ($L = I - O - \Delta S$) was estimated by ERA-Interim (or JRA-55) and three GRACE datasets (see blue and green circles, respectively). On the basis of the results from these nine groups of experiments, we finally inferred the multi-year average value of $L$ and performed the uncertainty analysis.

**Insert Figure S3 near here**

Specifically, uncertainties of annual water leakage $L$ were propagated from both modelling data ($P - E$ and $I - O$) and satellite observations ($\Delta S$). The standard derivation of yearly $L$ ( $\delta_L$) was calculated as

$$\delta_L = \sqrt{\delta_m{}^2 + \delta_s{}^2} \tag{6}$$

where $\delta_m$ denotes standard derivation from modelling data (i.e., GLDAS, ERA-Interim and JRA-55), while $\delta_s$ is one from GRACE satellites (CSR, JPL and GFZ).

Importantly, a critical effort towards quantifying the uncertainties of long-term annual average water leakage was also made in our analysis. Multiple error sources produced by the nine groups of modelling experiments (3 models $\times$ 3 GRACE solutions) were identified to propagate the uncertainties, which were then used to infer the 95% confidence intervals for long-term annual average water leakage ($\bar{L}$). We used following Eq. 7 and 8 to calculate the confidence intervals.

$$T = \frac{\bar{L} - \mu}{S/\sqrt{n}} \sim t(n - 1) \tag{7}$$

where $\bar{L}$ denotes the long-term annual average water leakage; $\mu$ is the mathematical expectation of normal distribution; $S$ is the standard derivation of experimental samples; $t$ means the statistical variable of $T$ obeys the $t$ distribution; $n$ is the number of samples (135 in this calculation).

$$\mu = \bar{L} \pm t_{\frac{\alpha}{2}}(n-1)S/\sqrt{n} \tag{8}$$

where the meaning of symbols is same as that in Eq. 7; The calculation of the 95% confidence intervals suggests 1- $\alpha$ = 0.95, and then the value of $t_{\frac{\alpha}{2}}(n-1)$ can be obtained by looking up the $t$ distribution table.

Based on the 135 experimental data (corresponding to the colour circles in Fig. S3), the long-term averaged value of $L$ is calculated to be $76 \pm 5$ mm yr$^{-1}$, giving a total excess of $54 \pm 4$ km$^3$ yr$^{-1}$ (uncertainties are in the 95% confidence intervals) in the water budget over the Qiangtang Basin.

## 6. Calculation of runoff coefficients for the upstream catchments of the Yarlung-Zangbo River

Two upstream catchments of the Yarlung-Zangbo River were considered as shown in Figure S4, i.e., Lazi Basin (No. 1 basin; 50,432 km$^2$) and Yangcun Basin (No. 2 basin; 106,376 km$^2$).

**Insert Figure S4 near here**

To calculate the runoff coefficient, $RC$ (the ratio of total annual precipitation across the catchment to total runoff, with runoff calculated as the total annual river discharge from the catchment less the total annual river inflow into the catchment), for both catchments, we collected from various sources data of observed annual precipitation and annual runoff for Lazi Basin and Yangcun Basin over the period of 1980-2010. The precipitation data were obtained from the Chinese monthly gridded precipitation (CMGP, 0.5º × 0.5º) dataset developed by the National Meteorological Information Center of the China Meteorological Administration (CMA) (Zhao et al., 2014). The high-quality CMGP dataset, starting from 1961, was produced from 2472 meteorological stations of Mainland China using the Thin Plate Spline (TPS) interpolation method (Zhao et al., 2014). The discharge data come from

the Chinese Hydrology Almanac books edited by the Chinese Ministry of Water Resources (CMWR) for the period of 1980-1999 and from the Tibet Hydrology and Water Resources Survey Bureau for the period of 2000-2010. The results show that the average $RC$ over the period considered is 0.39 for Lazi Basin and 0.56 for Yangcun Basin, respectively (Fig. S5).

**Insert Figure S5 near here**

The Nyang Qu and Lhasa rivers are two major tributaries of the Yarlung-Zangbo River, both within the Yangcun Basin (Figure S4). The $RC$ for Nyang Qu River (Dunzhu, 2015), which is intersected by the Yadong-Gulu Rift, is as low as 0.248. In contrast, the $RC$ for Lhasa River (Wen et al., 2002), which is not intersected by any rift, is 0.7, a typical value for 'normal' catchments.

**7. Analysing the water surface variations of the Duoqing Co lake in the Yadong-Gulu Rift south of the Yarlung-Zangbo River following a nearby earthquake**

Images from Landsat 8 Enhanced Thematic Mapper (ETM+) via the United States Geological Survey Earth Explore website (https://glovis.usgs.gov/, last accessed on 15 May 2019) were used to analyse the water surface variations of the Duoqing Co lake. Three bands of ETM+ including band 4 (red), band 3 (green) and band 2 (blue) were combined to generate the RGB images with a spatial resolution of 30 m. A total of 21 images were selected from the period between November 2015 and August 2016 and analysed to show how the lake responded to a nearby M3.7 earthquake that occurred on 14 February 2016 (epicentre: N27.0333, E89.1686). Figure 4 in the main text shows clearly the changes of the lake surface area from shrinking to drying up in response to the earthquake.

Using seven precipitation products including GLDAS, TMPA, CMORPH, GSMaP, PERSIANN, ITPCAS and CMGP, we calculated the monthly precipitation rates for the

Duoqing Co lake from November 2015 to August 2016 (Fig. S6). The relatively large rainfall in July 2016 filled up the lake, which was still largely dry in early July 2016 (Wu et al., 2018) but became mostly filled in 8 August 2016 (Figure 4F). The sequence of changes indicated initially leakage of lake water through tensional fractures that formed after the earthquake, and subsequently recovery of the lake as the fractures closed and heavy rainfall started.

**Insert Figure S6 near here**
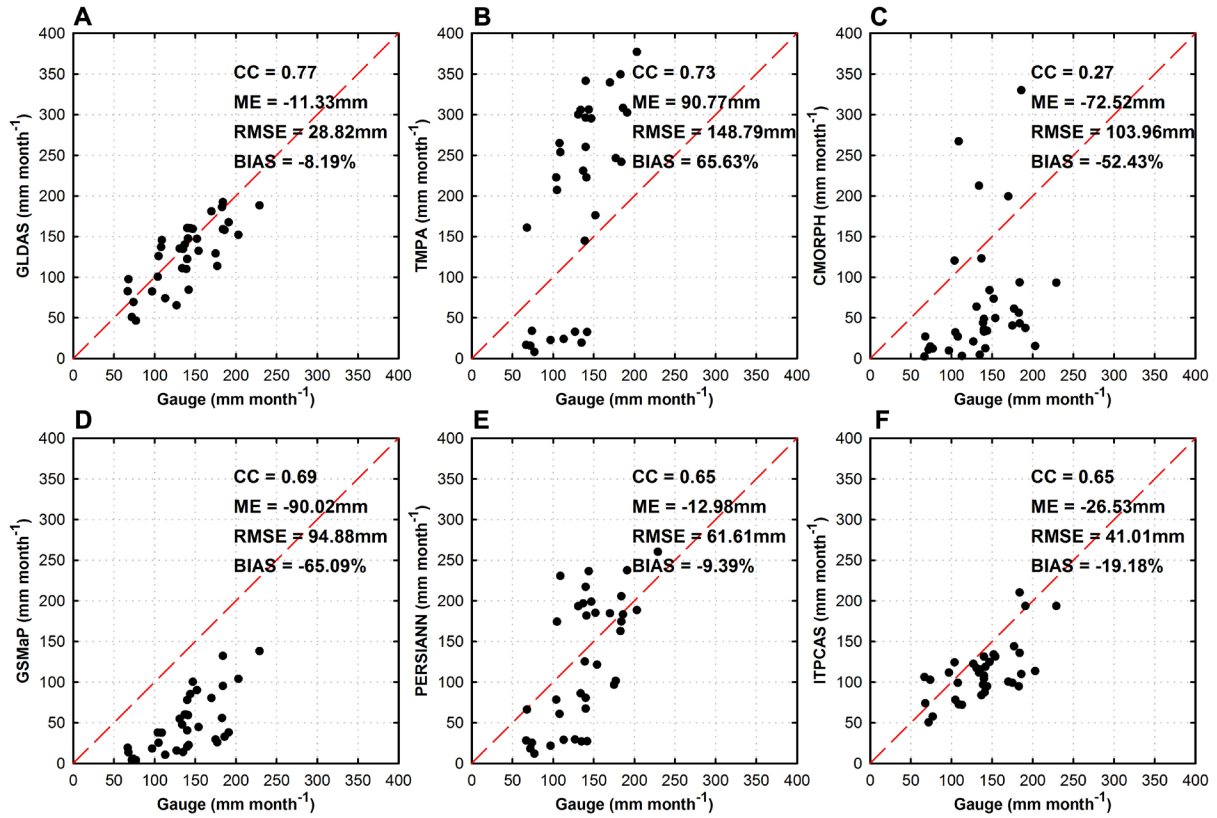
**Figure S1. Comparison of GLDAS precipitation and other satellite precipitation products.** Scatterplots of monthly precipitation estimates for (**A**) GLDAS, (**B**) TMPA, (**C**) CMORPH, (**D**) GSMaP, (**E**) PERSIANN and (**F**) ITPCAS against in situ observations from the nine rainfall gauges (Zhou et al., 2013) distributed in the southeast part of Qiangtang Basin. Note: The formulas and meaning of four statistical indices including Pearson linear correlation coefficient (CC), mean error (ME), root mean squared error (RMSE), and relative bias (BIAS) in each plot are described in more detail in Table 1 of Yong et al., (2010).
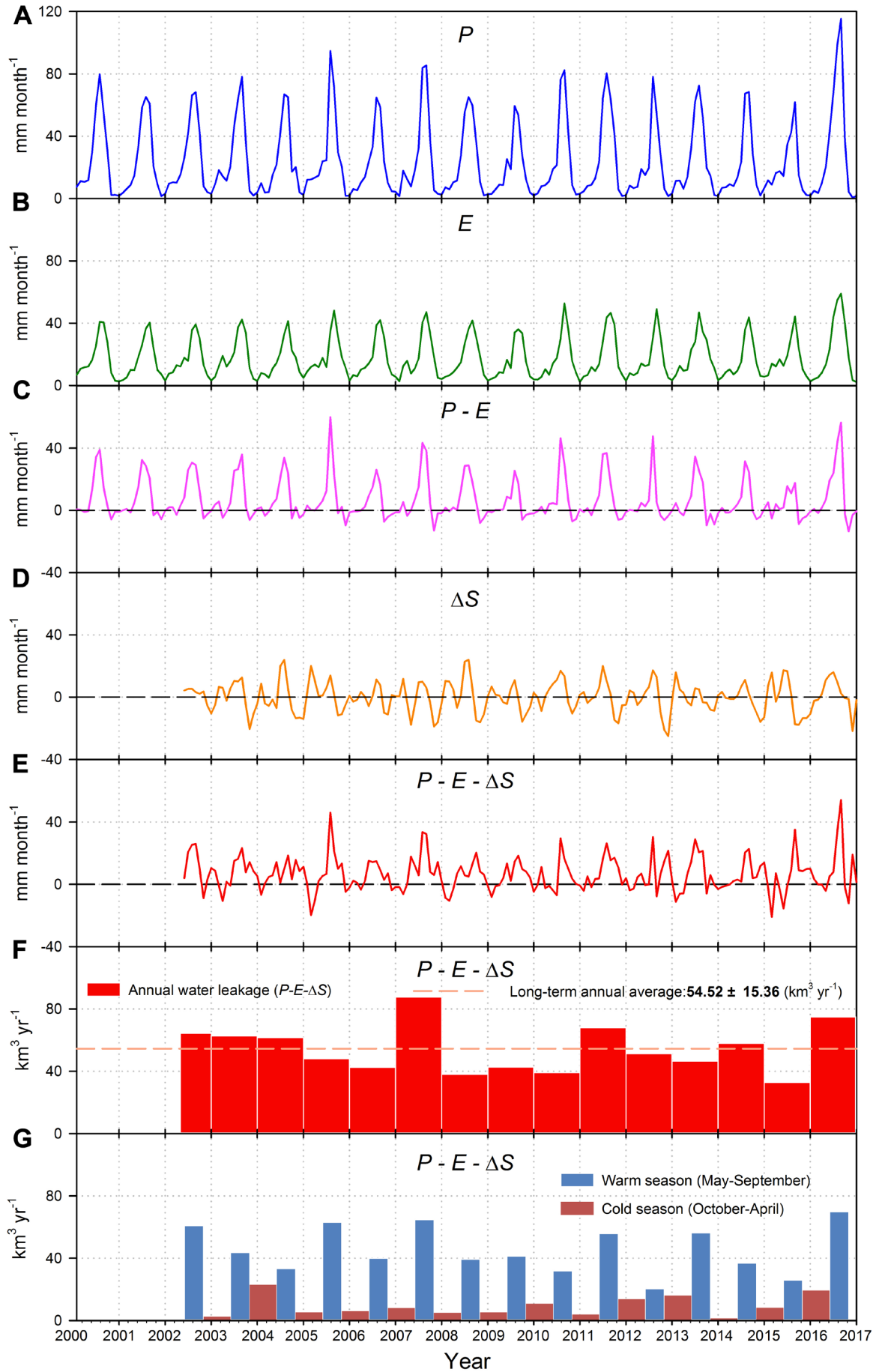
**Figure S2. Estimation of water leakage from Qiangtang Basin using the GLDAS and GRACE data.** Time series of monthly variations of (**A**) precipitation ($P$), (**B**) evapotranspiration ($E$), (**C**) $P - E$, (**D**) water storage change ($\Delta S$) from GRACE, (**E**) water leakage ($P - E - \Delta S$), (**F**) Annual amount of water leakage and (**G**) seasonal variations of water leakage. Blue bars indicate the amounts of water leakage during warm seasons (May-September); red bars show the amounts of water leakage during cold seasons (October-April).
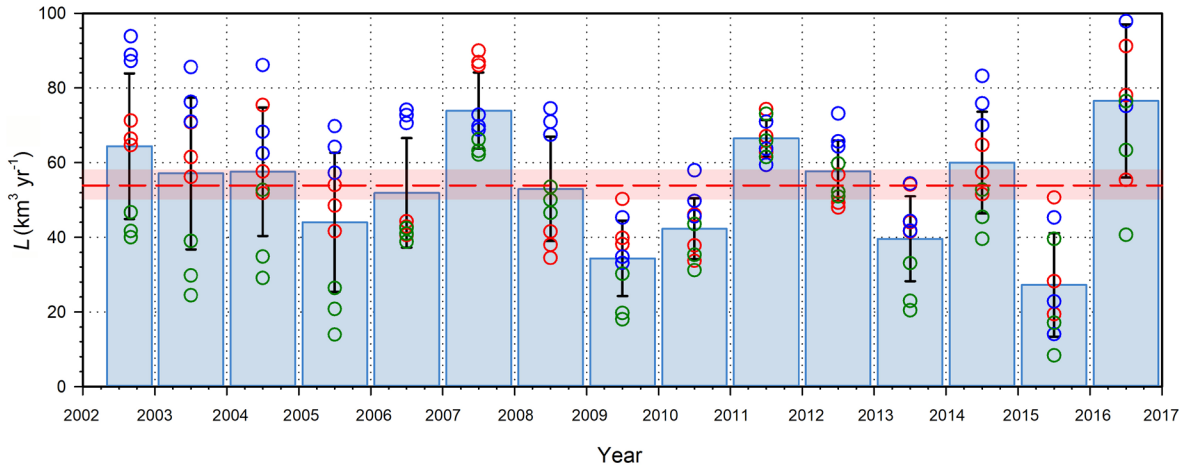
**Figure S3. Same as Figure 2D but showing all the values of annual water leakage (*L*)**

**computed from nine groups of modelling experiments (see above 135 circles).** Red

circles represent annual water leakage *L* = *P* – *E* – *ΔS* estimated by three groups of modelling

experiments, i.e., combining GLDAS and three GRACE satellite retrieval solutions (CSR,

JPL and GFZ), respectively. Blue (green) circles indicate annual water leakage *L* = *I* – *O* –

*ΔS* estimated by ERA-Interim (JRA-55) and three GRACE solutions. Dash line shows the

long-term average of the water leakage in the studied period. Transparent shades illustrate 95%

confidence intervals. Error bars represent standard derivation.
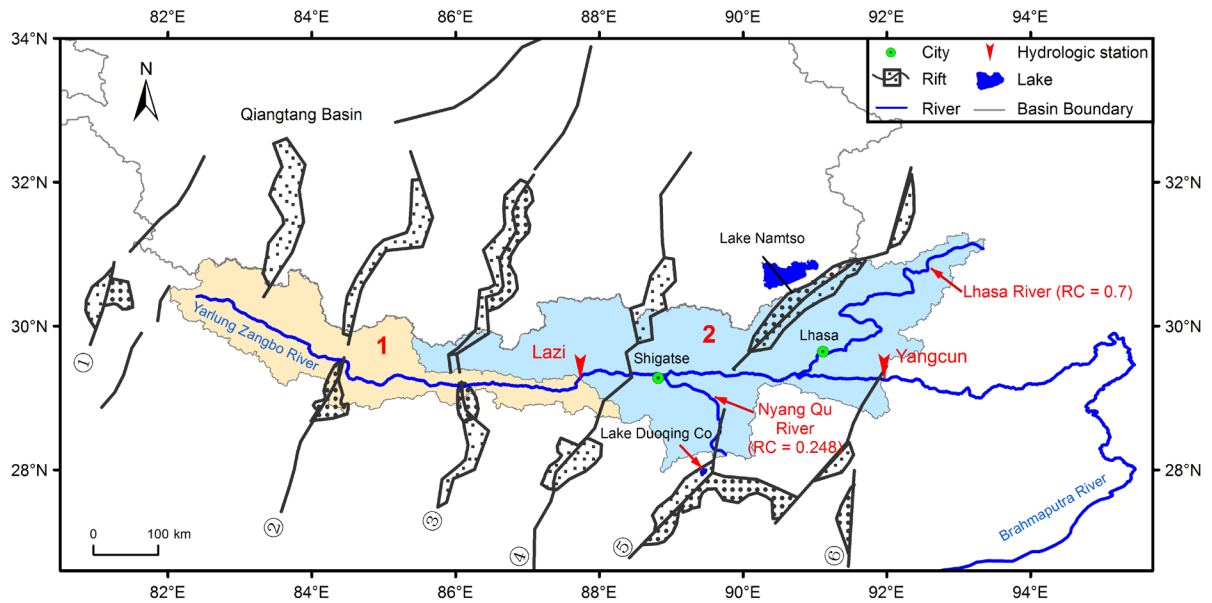
**Figure S4. Distribution of the Yarlung-Zangbo upstream basins and major rifts.**

Numbers 1 and 2 correspond to Lazi Basin (light yellow zone) and Yangcun Basin (light blue zone), respectively. Note that the Nyang Qu River with runoff coefficient (*RC*) of 0.248 (Dunzhu, 2015) stretches across the Yadong-Gulu Rift, while the Lhasa River with *RC* of 0.7 (Wen et al., 2002) does not overlap any rift. Numbers in circles locate different rifts (same as Figure 3).
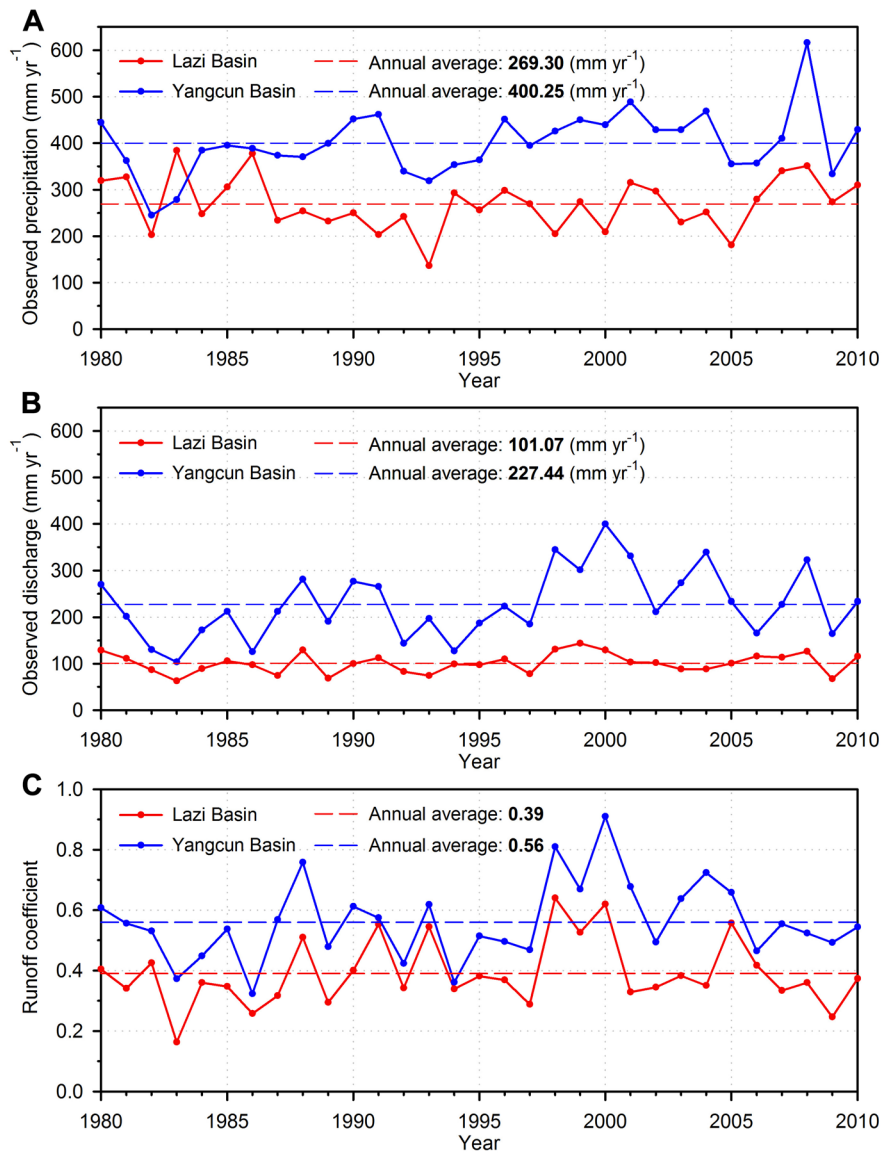
**Figure S5. Observed annual precipitation and annual runoff for Lazi Basin and Yangcun Basin during 1980-2010.** Annual variations of (**A**) observed precipitation, (**B**) observed discharge, and (**C**) runoff coefficient (*RC*).
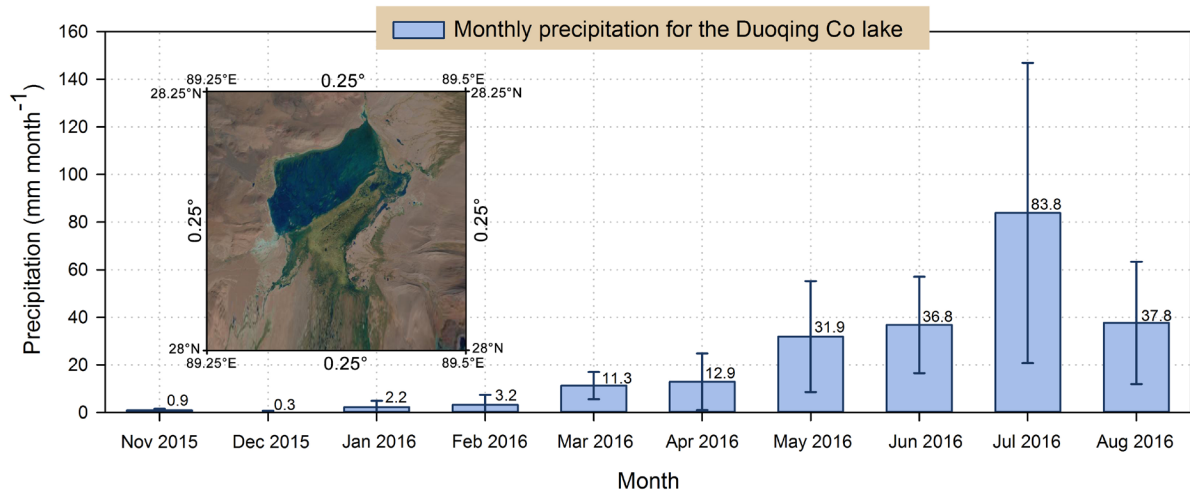
**Figure S6. Monthly precipitation data series for the Duoqing Co lake from November 2015 to August 2016.** The averaged monthly precipitation data on a 0.25°×0.25° grid (see insert) covering the Duoqing Co lake are computed from seven precipitation products including GLDAS, TMPA, CMORPH, GSMaP, PERSIANN, ITPCAS, and CMGP (error bars, one standard derivation).

**Data availability**

- The GLDAS (Noah V2.1) data are available from:

  https://disc.gsfc.nasa.gov/datasets?keywords=GLDAS.

- The ERA-Interim data can be downloaded at:

  https://apps.ecmwf.int/datasets/data/interim-full-daily/levtype=pl/.

- The JRA-55 data can be downloaded at:

  ftp://ds.data.jma.go.jp/?tdsourcetag=s_pcqq_aiomsg.

- The three GRACE resolutions are available on the JPL website:

  ftp://podaac-ftp.jpl.nasa.gov/allData/tellus/L3/land_mass/RL05/.

- The raw CMGP dataset is available at the website of the National Meteorological

  Information Center of China:

  https://data.cma.cn/data/cdcdetail/dataCode/SURF_CLI_CHN_PRE_MON_GRID_0.5.ht

  ml.

- The satellite-based precipitation products used in this study come from the following

  websites:

  TMPA is available from https://pmm.nasa.gov/data-access/downloads/trmm.

  CMORPH is available from ftp://ftp.cpc.ncep.noaa.gov/precip/global_CMORPH.

  GSMaP is available from ftp://rainmap:Niskur+1404@hokusai.eorc.jaxa.jp.

  PERSIANN is available from ftp://persiann.eng.uci.edu/pub/PERSIANN.

  ITPCAS is available from http://westdc.westgis.ac.cn/data.

- The ETM+ data were accessed via the United States Geological Survey Earth Explore

  website: https://glovis.usgs.gov/

**Additional Dataset S1**

Dataset S1.xlsx, contains the regional regional hydrological and meteorological data used to generate figures.

**References**

Andam-Akorful, S. A., Ferreira, V. G., Awange. J. L., Forootan, E., & He, X. (2015). Multi-model and multi-sensor estimations of evapotranspiration over the Volta Basin, West Africa. *International Journal of Climatology*, *35*, 3132-3145. https://doi.org/10.1002/joc.4198

Berrisford, P., Dee, D. P., Poli, P., Brugge, R., Fielding, M., Kallberg, M., et al. (2011). *The ERA-Interim archive Version 2.0*. https://www.ecmwf.int/en/elibrary/8174-era-interim-archive-version-20 (European Centre for Medium Range Weather Forecasts, ERA report series).

Cazenave, A., & Chen, J. (2010). Time-variable gravity from space and present-day mass redistribution in the Earth system. *Earth Planetary Science Letters*, *298*, 263-274. https://doi.org/10.1016/j.epsl.2010.07.035

Chen, Y., Yang, K., He, J., Qin, J., Shi, J., Du, J., & He, Q. (2011). Improving land surface temperature modelling for dry land of China. *Journal of Geophysical Research*, *116*, D20104. https://doi.org/10.1029/2011JD015921

Deber, J. C., Parrish, D. F., & Lord, S. J. (1991). The new global operational analysis system at the National Meteorological Center. *Weather Forecasting*, *6*, 538-547. https://doi.org/10.1175/1520-0434(1991)0062.0.CO;2

Ferreira, V. G., Montecino, H. D. C., Yakubu, C. I., & Heck, B. (2016). Uncertainties of the Gravity Recovery and Climate Experiment time-variable gravity-field solutions based on

three-cornered hat method. *Journal of Applied Remote Sensing*, *10,* 015015. https://doi.org/10.1117/1.JRS.10.015015

https://doi.org/10.1175/1525-7541(2001)002<0036:GPAODD>2.0.CO;2

Huffman, G. J., Adler, R. F., Morrissey, M. M., Bolvin, D. T., Curtis, S., Joyce, R., et al. (2001). Global precipitation at one-degree daily resolution from multisatellite observations. *Journal of Hydrometeorology*, *2*, 36-50.

Huffman, G. J., Bolvin, D. T., Nelkin, E. J., Wolff, D. B., Adler, R. F., Gu, G., et al. (2007). The TRMM Multisatellite Precipitation Analysis (TMPA): Quasi-global, multiyear, combined-sensor precipitation estimates at fine scales. *Journal of Hydrometeorology*, *8*, 38-55. https://doi.org/10.1007/978-90-481-2915-7_1

Jean, Y., Meyer, U., & Jäggi. A. (2018). Combination of GRACE monthly gravity field solutions from different processing strategies. *Journal of Geodesy*, *92,* 1313-1328. https://doi.org/10.1007/s00190-018-1123-5

Joyce, R. J., Janowiak, J. E., Arkin, P. A., & Xie, P. (2004). CMORPH: A method that products global precipitation estimates from passive microwave and infrared data at high spatial and temporal resolution. *Journal of Hydrometeorology*, *5*, 487-503. https://doi.org/10.1175/1525-7541(2004)005<0487:camtpg>2.0.co;2

*JRA-55 Product Users' Handbook.* (2013). http://jra.kishou.go.jp/JRA-55/document/JRA-55_handbook_LL125_en.pdf (Climate Prediction Division Global Environment and Marine Department, Japan Meteorological Agency).

Kubota, T., Shige, S., Hashizume, H., Aonashi, K., Takahashi. N., Seto, S., et al. (2007). Global precipitation map using satellite-borne microwave radiometers by the GSMaP project:

Production and validation. *IEEE Transactions on Geoscience and Remote Sensing*, *45*, 2259-2275. https://doi.org/10.1109/tgrs.2007.895337

Liu, G., & Zhou, Y. (1985). Water vapour transport over the mainland of China. *J. Hydraulic Engineering*, 11, 1-14. https://doi.org/10.13243/j.cnki.slxb.1985.11.001

Ramillien, G., Frappart, F., Güntner, A., Ngo-Duc, T., Cazenave, A., & Laval, K. (2006). Time variations of the regional evapotranspiration rate from Gravity Recovery and Climate Experiment (GRACE) satellite gravimetry. *Water Resources Research*, *421*, W10403. https://doi.org/10.1029/2005WR004331

Rodell, M., & Famiglietti, J. S. (1999). Detectability of variations in continental water storage from satellite observations of the time dependent gravity field. *Water Resources Research*, *35*, 2705-2723. https://doi.org/10.1029/1999wr900141

Rodell, M., Famiglietti, J. S., Wiese, D. N., Reager, J. T., Beaudoing, H. K., Landerer, F. W., & Lo, M. H. (2018). Emerging trends in global freshwater availability. *Nature*, *557*, 651-659. https://doi.org/10.1038/s41586-018-0123-1

Rui, H., & Beaudoing, H. (2018). *Readme document for GLDAS Version 2 data products.* https://hydro1.gesdisc.eosdis.nasa.gov/data/GLDAS/GLDAS_NOAH025_M.2.1/doc/READ ME_GLDAS2.pdf (NASA Goddard Space Flight Centre, Report number 610.2, last revised 29 March 2018).

Scanlon, R., Zhang, Z., Save, H., Sun, A. Y., Schmied, H. M., van Beek, L. P. H., et al. (2018). Global models underestimate large decadal declining and rising water storage trends relative to GRACE satellite data. *P* https://doi.org/*roceedings of National Academy of Sciences of the United States America*, *115*, 1080-1089. 10.1073/pnas.1704665115

Sorooshian, S., Hsu, K., Gao, X., Gupta, H. V., Imam, B., & Braithwaite D. (2000). Evaluation of PERSIANN system satellite-based estimates of tropical rainfall. *Bulletin of the American Meteorological Society*, *81*, 2035-2046. https://doi.org/10.1175/1520-0477(2000)0812.3.CO;2

Starr, V. P., & White, R. M. (1954). *Balance requirements of the general circulation*. (Cambridge, Mass, Geophys. Res. Directorate, Air Force Cambridge Research Center).

Swenson, S. C. (2012). *GRACE monthly land water mass grids NETCDF, RELEASE 5.0*. http://dx.doi.org/10.5067/TELND-NC005 (US NASA JPL).

Tapley, B. D., Bettadpur, S., Watkins, M., & Reigber, C. (2004). The gravity recovery and climate experiment: mission overview and early results. *Geophysical Research Letters*, *31*, L09607. https://doi.org/10.1029/2004GL019920

WMO/IHD Projects Report. (1973). *Atmospheric vapour flux computation for hydrological purposes*. (No. 20, WMO-No. 357, Geneva).

Yong, B., Ren, L., Hong, Y., Wang, J., Gourley, J. J., Jiang, S., et al. (2010). Hydrologic evaluation of Multisatellite Precipitation Analysis standard precipitation products in basins beyond its inclined latitude band: A case study in Laohahe basin, China, *Water Resources Research*, *46*, W07542. https://doi.org/10.1029/2009WR008965

Zhao, Y., Zhu, J., & Xu, Y. (2014). Establishment and assessment of the grid precipitation datasets in China for recent 50 years. *Journal of Meteorological Sciences*, *34*, 414-420. https://doi.org/10.3969/2013jms. 0008 (in Chinese with English abstract)